International Journal of Engineering Research and Development
e-ISSN: 2278-067X, p-ISSN: 2278-800X, www.ijerd.com
Volume 8, Issue 10 (October 2013), PP. 45-57

Diffeomorphic MRI-Brain Registration Using Mean-Shift Algorithm

R.Mythili1, S.Gowthami2
[1]*M.E-Student, Department of CSE, Kongunadu College of Engineering and Technology, Tamil Nadu, India.*
[2]*Asst. Professor, Department of CSE, Kongunadu College of Engineering and Technology, Tamil Nadu, India.*

Abstract:- A new methods to constrain brain MRI registration, and perform experiments evaluating the alignment of manually-traced structures, reduction of intersubject variance, and morph metric results using group wise registration is compared against traditional MRI. By using image registration, it restrict the scope of structures to those that can be represented volumetrically as images, such as MRI volumes or anatomical segmentations, or those that can be interpolated on a volumetric grid.This method uses Mean Shift algorithm to efficiently segment the gray and white matter.

Keywords:- Atlases morphometry, brain registration, diffeo- morphisms, MRI.

I. INTRODUCTION

WHOLE brain image registration is a useful and often necessary tool for studying morphometry and pooling information in a central space. Registration can be a diffi- cult task considering the anatomical variability and structural complexity present in the human brain, motivating the use of structure-specific information (anatomical guidance) to initial- ize and constrain registration in a meaningful way. We described how individual brain structures could be used to per- form an initial low- and high-dimensional alignment, leading to improved registration of specific subregions in the brain. More direct shape-matching approaches have shown that using manually traced segmentations to drive the registration instead of MRI intensities can also improve registration of specific corti- cal and neocortical regions. The main contribution of this study is a registration framework that concurrently employs shape- matching with automated segmentations of multiple structures, and image-matching to obtain an anatomically guided diffeo- morphic registration that can more accurately align the individ- ual structures in images.

Previous work integrating registration and segmentation can be categorized into those that perform the tasks simultaneously, and those that perform the tasks in sequence. Simultaneous, or joint segmentation and registration approaches are attractive because they model the inherent interdependence of each component. However, because of limitations in how the segmentation and registration models can be simultaneously optimized, these methods have not been able to take advantage of more sophisticated or specialized approaches. In contrast, by employing registration and segmentation sequentially, where the contribution becomes how one applies the results of one to aid the other, specialized and potentially disparate techniques, such as surface-based and volume-based segmentation, can be combined to provide a more accurate result. We exploit this idea in this study by making use a segmentations derived from a sophisticated image analysis pipeline employing surface-based registration, namely Freesurfer, and use these to drive a highly deformable large-deformation diffeomorphic registration algorithm. Thus, conceptually the multistruc- ture registration could be thought of as a refinement iteration where a full 3-D diffeomorphism is found using the label con- straints generated via an earlier iteration of lower dimensional and surface-based registration techniques.

A key component of many group-based neuroanatomical studies is the extraction of morphometric features that can be used for discrimination or characterization of anatomical variability within or across groups. Whole brain morphometry approaches, such as voxel-based and tensor-based morphom- etry (TBM) compute morphometric features at a voxel-wise level, which can then be used in mass-univariate or multivariate statistical analyses. Tensor-based morphometry makes use of the transformations obtained from registration to measure the amount of deformation required to match a subject's anatom- ical features to a template. A subject that is morphologically very different would require a greater amount of deformation in registration to match the template, whereas a subject morpho- logically similar to the template would require less deforma- tions. Since the sensitivity of TBM inherently depends on how accurate the underlying registration algorithms are, we also in- vestigate how our proposed registration methods perform when applied to TBM.

We begin by introducing our multistructure registration framework, then describe a groupwise implementation for av- erage atlas building. We then describe how Freesurfer segmentation. structure segmentation, we have the energy functional for our multistructure registration

$$(\nabla_v E_t)_V = 2v_t - 2K\left(|D\phi_{t,1}|\left[\lambda^{\mathrm{MR}}\left(\tilde{I}^{\mathrm{MR}}_{a,t} - \tilde{I}^{\mathrm{MR}}_{b,t}\right)\nabla \tilde{I}^{\mathrm{MR}}_{a,t} + \sum_{i=1}^{N}\lambda^{\mathrm{Seg},i}\left(\tilde{I}^{\mathrm{Seg},i}_{a,t} - \tilde{I}^{\mathrm{Seg},i}_{b,t}\right)\nabla \tilde{I}^{\mathrm{Seg},i}_{a,t}\right]\right) \quad (3)$$

II. METHODS

2.1 Multistructure Registration

Diffeomorphic registration algorithms that ensure the result- ing transformations are one to one, invertible and smooth, are desirable because they preserve the topological properties of the underlying anatomy. We employ a large defor- mation diffeomorphic registration algorithm in this study for these reasons; however, it is possible to implement the proposed

Now, we have additional weights $\lambda^{\mathrm{Seg},i}$ specifying the relative influence of each segmentation in the overall registration. In this study, we chose equal weights, and thus equal contribution for all segmentations and the MRI, $\lambda^{\mathrm{MR}} = \lambda^{\mathrm{Seg},i}, i = 1 \ldots N$. Note that by employing structure segmentations in the energy functional as such, point correspondences between segmented volumes do not have to be found, since it is effectively the boundary differences that drive the deformations.

The Euler–Lagrange equations for this energy minimization problem are

$$E(v) = \int_0^1 \|v_t\|_V^2 \,\mathrm{d}t + \lambda^{\mathrm{MR}}\|I_a^{\mathrm{MR}} \circ \phi_{1,0} - I_b^{\mathrm{MR}}\|_{L^2}^2 + \sum_{i=1}^{N}\lambda^{\mathrm{Seg},i}\|I_a^{\mathrm{Seg},i} \circ \phi_{1,0} - I_b^{\mathrm{Seg},i}\|_{L^2}^2.$$

Typically, the registration is driven by the intensities of the anatomy, and has been shown to better align regions such as the medial temporal lobe . In our multistructure registration framework, we add a number of shape-matching terms, each

V is a compact self-adjoint operator defined by $a, b_L{}_2 = Ka, b_V$, such that for any smooth vector field $\boldsymbol{f} \epsilon V$, $K(L^{\dagger}L)\boldsymbol{f} = \boldsymbol{f}$ is satisfied [12]. The operator L is chosen

2

corresponding to a segmentation of a volumetric structure, andto be of the Cauchy–Navier type, $L = -\alpha\nabla$

$+ \gamma \boldsymbol{I}$, where $\boldsymbol{I}$ is

2 ∂^2

∂^2 ∂^2

register all of these structure channels simultaneously along with

the identity operator and ∇

$= \partial x^2 + \partial y^2 + \partial z^2$ is the Lapla-

the MRI. We now describe how the large deformation diffeo-

morphic formulation was extended toward multistructure registration.

cian operator.

Let the pair $\boldsymbol{I}^{\mathrm{MR}}$

and $\boldsymbol{I}^{\mathrm{MR}}$

of whole brain MR images

be given, and let segmentations of N structures, $\boldsymbol{I}^{\mathrm{Seg},i}, i \epsilon$

$[1, \ldots, N]$, and $\boldsymbol{I}^{\mathrm{Seg},i}, i \epsilon$

$[1, \ldots, N]$,

be available. The dif-

feomorphic transformation matching $\boldsymbol{I}_a$

and $\boldsymbol{I}_b$

is given by

$\phi : \Omega \rightarrow \Omega$ such that $I_a \circ \phi^{-1} \approx I_b$. This transformation ϕ is built from the flow of smooth time-dependent velocity vector field, $v_t \in V, t \in [0, 1]$, where V is a Hilbert space of smooth,compactly supported vector fields on Ω. Such a velocity vector field defines the evolution of a curve $\varphi_{0,t}, t \in [0, 1]$ via the evolu tion equation $\dot{\varphi}_{0,t} = v_t(\varphi_{0,t})$ such that the end point $\varphi_{0,1}$ of the curve φ at time $t = 1$ is the particular transformation $\phi = \varphi_{0,1}$that is sought for registration. Let the notation $\varphi_{s,t} : \Omega \rightarrow \Omega$denote the composition $\varphi_{s,t} = \varphi_t \circ (\varphi_s)^{-1}$ with the interpretation that $\varphi_{s,t}(y)$ is the position at time t of a particle that is atposition y at time s. Hence, the transformed image I_a is given by $I_a \circ \phi^{-1} = I_a \circ \varphi_{1,0} \approx I_b$ and the transformed target im- age is $I_b \circ \varphi_{0,1}$.

Here, the weight λ^{MR} enforces how much mismatch in the images is penalized. Adding additional matching terms for each

This can be extended to the multistructure case, LDDMM- MultiStruct, by including additional terms for multiple struc- tures.

Using the optimizer then becomes $v_t = -K(b_t)$, which can be integrated to compute the map $\varphi_{t,0}$.

2.2 Groupwise Multistructure Registration

When applying pairwise registration to spatially normalize all subjects to a given template, one has to decide which subject to choose as the template. The choice of template also affects how well the pairwise registrations perform, as subjects that are more similar to the template will likely be registered better. To avoid choosing a template, groupwise, or unbiased approaches have been proposed in the past , where the central template is generated and represented as an average of the group. One natural way to define a central template is using the Fréchet mean, where the intrinsic mean of a set of data points x_i is de- fined as the point $\bar{x}$ that minimizes the sum of squared distances to each data point

$$\bar{x} = \operatorname{argmin} \sum_{x \in X}^{M} d(x, x_i)^2 .$$

Input: Set of multi-structure images $\mathbf{I}_1, \mathbf{I}_2, \ldots, \mathbf{I}_M$;
Multi-scale smoothing schedule: $\{\alpha_k, \gamma_k\}$
Output: Ensemble average multi-structure image $\bar{\mathbf{I}}$
Set $\varphi_j^{(0)} = id$;
for $k = 0$ *to* N_k **do**
  $\bar{\mathbf{I}}^{(k)}(x) = \frac{\sum_{j=1}^{M} |D(\varphi_j^{(k)})| \mathbf{I}_j \circ \varphi_j^{(k)}(x)}{\sum_{j=1}^{M} |D(\varphi_j^{(k)})|}$;
  foreach $\mathbf{I}_j$ **do**
    Compute $\varphi_j^{(k+1)}$ using the body force from equation (6), using differential operator: $L_k = -\alpha_k \nabla^2 + \gamma I$;
  end
end

Algorithm 1. Multi-structure group-wise average.

where $\bar{\mathbf{I}}$ is a multistructure image consisting of $\bar{I}^{\mathrm{MR}}$ and N structure-channels, $\bar{I}^{\mathrm{Seg},i}$. For 2) we use pairwise diffeomor- phic registration from $\mathbf{I}_j$ to the fixed average $\bar{\mathbf{I}}$ to obtain the maps ϕ_j. We used a multiscale smoothing schedule by succes- sively decreasing the viscosity parameter, α, in the fluid-flow differential operator L after each iteration. The sequence used was $\alpha = 2, 1, 0.5$, and 0.1, with a fixed $\gamma = 0.01$, which was chosen based on experiments quantifying effective smoothing to be equivalent to 20, 15, 10, and 5 mm effective smooth- ing.

2.3 Freesurfer Structure Segmentation

Extending this idea to the general problem of template estima- tion, the central template $\bar{I}$ thus becomes the image that requires the minimal deformation ϕ_i to match each image I_j in the set of images

In this section, we describe how we applied our multistruc- ture diffeomorphic registration to brain registration, where a set of initial segmentations were used as structures along with the MRI. Because we are using image registration, we thus re- strict our scope of structures to those that can be represented

$\{\bar{\phi}_j, \bar{I}$

$= \text{argmin} \quad E(I_j \circ \phi_j, I) + D(Id, \phi_j)^2 .$

$\phi_j \in G, I \in I \; {}_{j=1}$

volumetrically as images, such as MRI volumes or anatomical segmentations, or those that can be interpolated on a volumetric

We extend this idea to multistructure registration by computing the groupwise average subject, defined as the multistructure image $\bar{I}$ that has minimal distance to each image in the database surface-based atlas. The surface-based labels are mapped from

the atlas using the cortical folding patterns, specifically the cur- vature of the cortical surface, and are then converted to a volu-

metric representation by projecting the label values from the sur- face to the voxels labeled as cortical gray matter. The use of these

To solve for $\{\bar{\phi}_j, \bar{I}\}$

we use an alternating estimation proce-

structures from Freesurfer thus, provides the multistructure reg-

dure, where 1) $\bar{\phi}_j$ is fixed to find $\bar{I}$, and 2) $\bar{I}$ is fixed to find $\bar{\phi}_j$. For

1) when transforming the images into the average image space

we used the Jacobian to preserve the information regarding the volumes of structures, as was also done in [21], [22]

M

istration with constraints from a surface-based representation of the cortex, which is known to better represent anatomical struc- ture and function of the highly convoluted cortical topology. We used the following eight subcortical structures, left and right in- clusive: lateral ventricles, caudate nucleus, putamen, pallidum,

$\bar{I} =$

$\sum_{j=1} |D\phi_j| I_j \circ \phi_j$

$\sum_{j=1} |D\phi_j|$

nucleus accumbens, thalamus, hippocampus, and amygdala. For cortical structures, we used the following 34 labels, left and right inclusive: bankssts (banks around the superior temporal sulcus), caudal anterior cingulate, caudal middle frontal, corpus callo- sum, cuneus, entorhinal, fusiform, inferior parietal, inferior tem- poral, isthmus cingulate, lateral occipital, lateral orbito-frontal, lingual, medial orbito-frontal, middle temporal, parahippocam- pal, paracentral, pars opercularis, pars orbitalis, pars triangu- laris, pericalcarine, postcentral, posterior cingulate, precentral, rostral anterior cingulate, rostral middle frontal, superior frontal, superior parietal, superior temporal, supramarginal, frontal pole, temporal pole, and transverse temporal. Including the MRI as the first structure, we have 43 structure channels for each hemi- sphere making up our multistructure set.

The segmentation labels making up the multistructure set were extracted from the Freesurfer output images, namely

aparc+aseg.mgz, 1 mm isotropic voxels, $256 \times 256 \times 256$,

smoothed with a Gaussian filter ($\sigma = 2$). Smoothing was per-

formed to mitigate labeling and discretization errors commonly found on the boundaries of the Freesurfer segmentations. For each structure, the labels from both hemispheres were combined into a single image with unique intensities.

2.4.Initial Affine Registration and Intensity Normalization

Before performing the diffeomorphic multistructure regis- tration, the target subjects were first aligned using a 12-D affine transformation. The registration was performed on the

For pairwise registration, the bounding box was applied to the affine-registered target brain and multistructure set, and multistructure registration was carried out as described in Section II-A, with the parameters of the differential operator being $\alpha = 0.1$ and $\gamma = 0.01$.

For the group-wise approach, a template subject was initially chosen, all targets were affine registered to it, and the bounding box defined on it was applied to all targets. For the registration a multiscale smoothing scheme was used, which successively decreased the viscosity parameter α after each iteration. The sequence used was $\alpha = 2$, 1, 0.5, and 0.1, with a fixed $\gamma = 0.01$, which was chosen based on experiments quantifying effective smoothing to be equivalent to 20, 15, 10, and 5 mm effective smoothing.

2.6 ***Brain Registration Evaluation***

The goal of brain registration is to bring structures into align- ment with each other; thus, a commonly-used method to evaluate registration performance is to manually segment brain structures in a group of subjects, and measure how well the structures are aligned after registration. To use this label-agreement method of evaluation, we performed fully crossed pairwise brain regis- trations on a given dataset, that is, each subject I_j is registered to every other subject $I_{k=j}$ and compared the manual segmen- tations of this subject, I^{Manual} with the propagated manual seg-

Freesurfer tissue segmentation images of the template and tar- get, which have discrete values of (0, 85, 170, 255) for the mentations, $I^{Manual}{}_{\circ\varphi j,k}$.= background, cerebrospinal fluid, gray matter, and white mat- ter, respectively. The algorithm was implemented in the Insight Toolkit and used regular step gradient descent and a mean- squared error image metric with the transform initialized with the translation bringing the centers of mass into alignment. Once the transform was computed, the target MR images and Freesurfer labels were all transformed to the template space using this 12-parameter transformation and linear interpolation. To address MRI intensity nonstandardization, we performed

a piecewise linear intensity transformation of the target image, where the median white matter, gray matter, and cerebrospinal fluid intensities of the template and target image are used to define the transformation. These median intensities are found by masking the nonuniformity corrected MRI images with the Freesurfer tissue segmentation images, which are first morpho- logically eroded to avoid voxels that may be susceptible to partial voluming.

2.5 Diffeomorphi Registration

To limit computational and memory requirements, we con- struct a bounding box around the template brain, and use this subvolume in registration instead of the entire $256 \times 256 \times 256$ volume. The bounding box is defined using the extents of the skull-stripped brain allowing for at least 16 voxels (16 mm) of padding at each boundary, and also ensuring the dimensions of the image are divisible by 16, such that this level of data paral- lelization could be used. The bounding box is applied to both the MRI and multistructure set of the template.

2.7Tensor-Based Morphometry

We applied TBM to investigate how well the multistructure and MRI-only registration methods can detect the expected dif- ferences between a group of demented patients and cognitively normal patients. Groupwise registration was carried out as de- scribed in the previous section to obtain transformations and log-determinant Jacobian maps from the average to each sub- ject.

The SurfStat package[1], is capable of random-field theory
analysis with general linear and multivariate modelling on both volumetric and surface data. In this software, the linear model is specified for example as

$$P = Group + Age + Gender$$

where *Age* and *Gender* are nuisance covariates in the model testing for group differences, obviating the need to specify a design matrix. We use SurfStat to generate statistical parametric maps for our TBM results using the log-determinant Jacobians.

III. MATERIALS

We used freely available MR imaging datasets to evaluate our brain registration methods. These datasets are available online to researchers, and provide an open repository for data sharing and method comparison.

The Internet brain segmentation repository (IBSR) 1.5T Dataset consists of 18 healthy controls, provided by the Center for Morphometric Analysis at Massachusetts General Hospi- tal. The ages of the subjects ranged from juvenile to 71 years. Manual segmentations were provided for 48 cortical regions.

The Laboratory of Neuro Imaging Probabilistic Brain Atlas (LPBA40) [24] consists of 40 healthy controls, provided by the University of California, Los Angeles Laboratory of Neuro Imaging. Subjects were scanned on a GE 1.5T scanner, with average age at time of acquisition 29.20 ± 6.30 (mean $\pm$ S.D.)
years (min = 19.3, max = 39.5 years). Manual segmentations of 56 structures, mainly cortical, were provided, with a manual segmentation protocol defined by Shattuck *et al.* [24].

These two datasets were recently used to evaluate brain reg- istration accuracy for 14 commonly used registration methods [25]. Note that two other smaller datasets (CUMC12, MGH10) were also used in that study; however, we only used the two largest datasets here. Since we used the same datasets, method- ology, and evaluation metrics as the Klein *et al.* evaluation, we can directly compare our results to the leading brain registration methods applied in that study. For evaluating group-wise average atlas construction and morphometry, we used MRI datasets from the Open Access Series of Imaging Studies (OASIS), freely available online (http://www.oasis-brains.org). We used baselines scans from a dataset consisting of 150 subjects, aged 60–96 years with 64 of the subjects characterized with very mild to mild Alzheimer's disease [26].

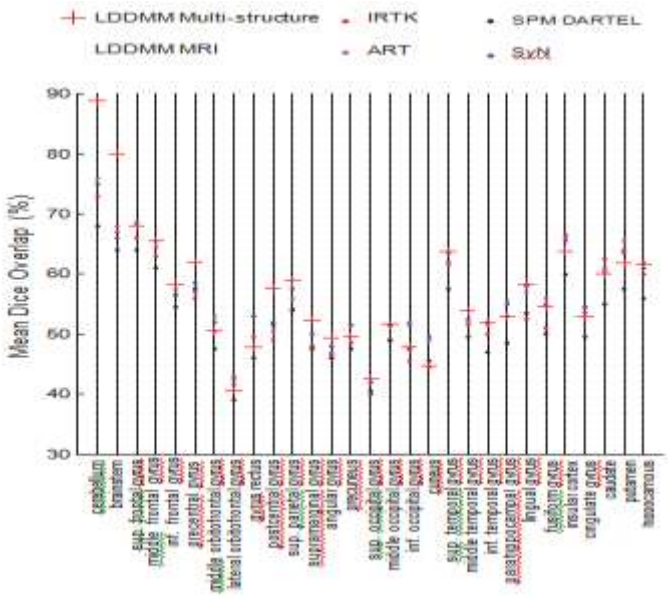

IV. RESULTS

4.1 Brain Registration Evaluation

Figs. 1 and 2 plot the Dice overlaps for the LPBA and IBSR datasets, averaged over all pairwise registrations in each dataset. Since we did not observe a significant difference between left and right structures, the mean dice scores for bilateral struc- tures were also averaged to summarize the results further. We compared locally optimal LDDMM registration using multi- structure (LDDMM Multistructure) and MRI-only (LDDMM MRI) costs against the four top ranked registration methods from the [25] evaluation: SyN [27], ART [28], IRTK [15], and SPM Dartel [29]. One of the most significant findings of that study was that the relative performances of the registration methods under comparison appear to be little affected by the choice of subject population, labeling protocol, and type of overlap mea- sure, thus our choice of only using the two largest datasets and the Dice overlap measure is justified.

On the LPBA dataset, we see that our multistructure approach improves accuracy over our MRI-based approach for nearly all structures, except for the gyrus rectus and lateral orbitofrontal gyrus, both located in the frontal lobe. The improvement is espe- cially notable in the hippocampus and postcentral gyrus, where the MRI-based method is the worst performing of the group and the multistructure method is one of the best performing. Comparing to the other methods, our Dice overlaps are gener- ally in the same range except for the cerebellum and brainstem, where both LDDMM and LDDMM MultiStruct are consider-

Fig. 1. Mean Dice overlap scores for each manually-traced structure (bilateral structures combined) from fully crossed pairwise registrations of the 40 subjects in the LPBA dataset (1600 pairwise registrations). Our locally optimal LDDMM registration with multistructure and MRI-based cost functions are compared against the top performing registration methods: SPM Dartel, SyN, IRTK, and ART.

ably higher. This could be attributed to the fact that our brains were not skull-stripped prior to registration, whereas [25] used the manual labels to generate a brainmask for skull-stripping; it is possible that the additional information in the neck aids in registration of the mid-brain regions.

For the IBSR dataset, we see multistructure generally has higher overlaps than MRI-based for most regions, except for the temporal pole, temporal gyrus, parietal lobule, supramarginal gyrus, frontal orbital gyrus, and Heschl's gyrus. The reduced performance in the frontal lobe was also seen in the LPBA dataset. Comparing to the other methods, our methods have higher overlaps for all structures. This is notable, since the IBSR dataset uses a different cortical labeling protocol which only includes the cortical gray matter in the label, whereas the LPBA labeling protocol uses gross-sized labels that can encompass CSF and white matter as well; thus, performance assessment on the IBSR dataset is more stringent since it penalizes mislabeling across tissue types.

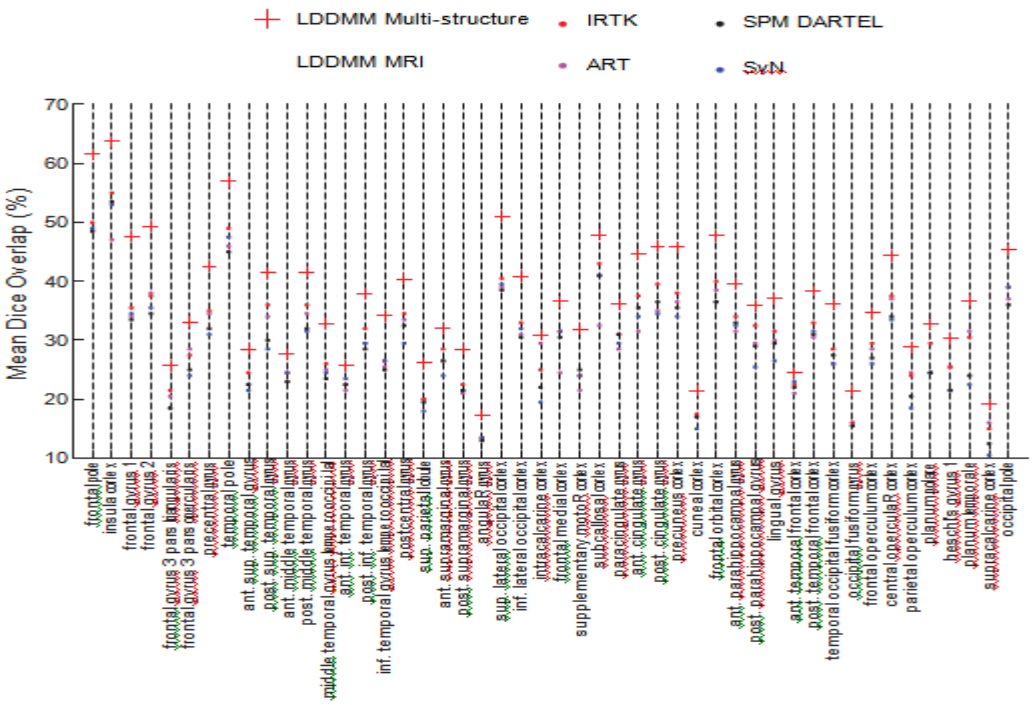

Fig. 2. Mean Dice overlap scores for each manually traced structure (bilateral structures combined) from fully crossed pairwise registrations of the 18 subjects in the IBSR dataset (324 pairwise registrations). Our locally optimal LDDMM registration with multistructure and MRI-based cost functions are compared against the top performing registration methods: SPM Dartel, SyN, IRTK, and ART.

4.2 Groupwise Average Atlas

To qualitatively evaluate the performance of our multistruc- ture and MRI-based groupwise average atlas generation, we performed them on the OASIS 150 subject set, generating an LDDMM MultiStruct average and an LDDMM MRI average. Fig. 3 shows representative axial slices of the average T1 MRI image, generated by transforming each subject's T1 MRI im- age to the average space, using the final mappings from the group-wise average, and performing voxel-wise averaging. In regions where the anatomy is not well aligned and thus has a mixture of different tissue types from the subjects, the image is effectively blurred. In contrast, where the anatomy is well aligned the anatomical boundaries are effectively sharper. We see here that the multistructure approach improves registration in many regions, especially cortical regions, as can be seen by the sharp and well-defined boundaries. To further investigate this effect, we transformed the gray matter segmentations from each subject to the average space to generate an average gray matter mask, as shown in Fig. 4. We see a similar pattern here,

with greater definition of cortical folding patterns in the average generated by multistructure registration. To further inspect alignment of cortical anatomy with our approaches, we performed a cortical surface reconstruction of the average MRI images using the Freesurfer image analysis suite. This processing also includes a cortical labeling using curvature-based surface registration to an atlas. Fig. 5 shows the cortical surface reconstructions for the average images from MRI-based and multistructure group-wise registration. Here, we see that the multistructure-based cortical surface shows much greater detail and consistency, closer to what one would see in an individual's cortical surface, demonstrating the superior alignment of cortical regions as compared to single-channel MRI-based registration.

We can quantify the alignment of these group-wise ap- proaches by computing the residual variance in the intensi- ties of the aligned MRI images. We computed the variance of prenormalized MRI intensities at each voxel, and thresholded at $\sigma = 20$ to generate a map that can be overlaid on the average

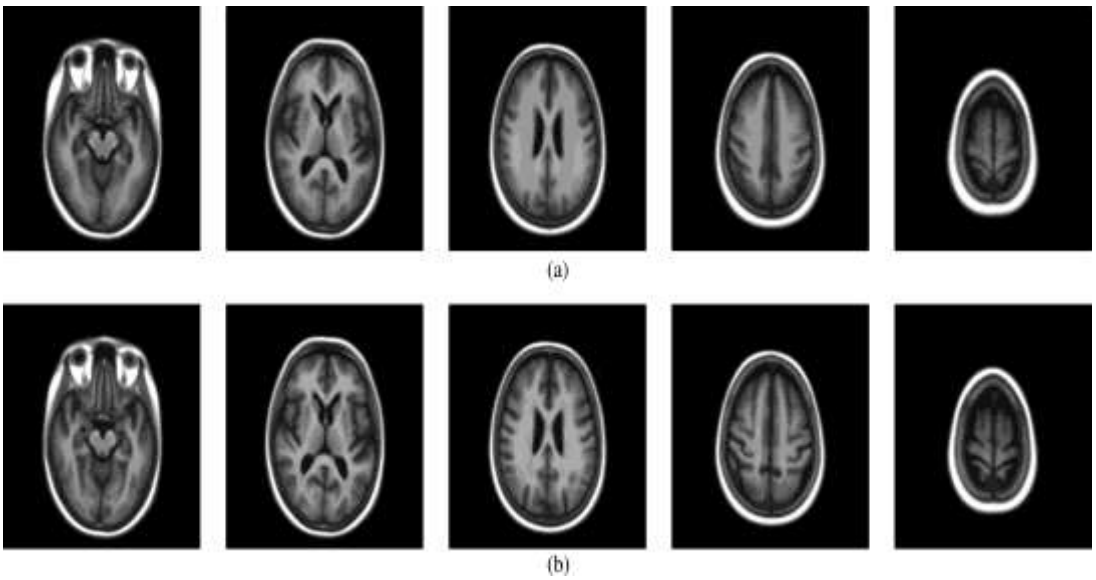

Fig.3. Average T1 MRI images from groupwise registration of all subjects in the OASIS database (150 subjects), comparing the average obtained via (a) MRI-based (single-channel) and (b) multistructure registration, both using locally optimal LDDMM registration. Registration performance can be assessed by whether the anatomical features are sharp (high accuracy) or blurred (low accuracy). Both methods show good alignment in the subcortical regions but the multistructure variant exhibits much better cortical alignment resulting in sharper delineation of cortical folds in the averaged brain MR image.

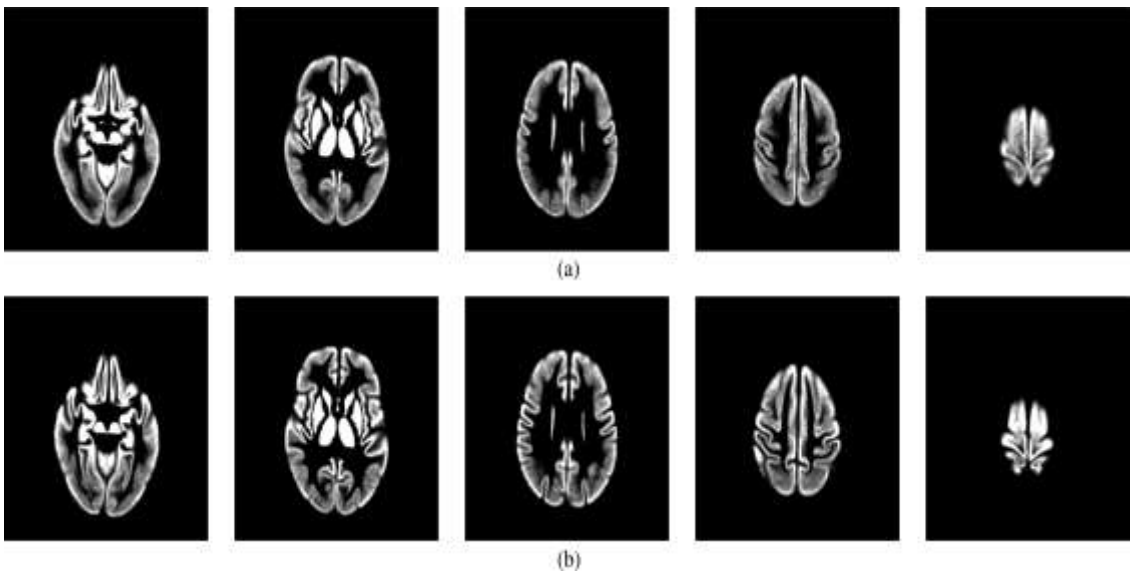

Fig. 4. Average gray matter segmentations from groupwise registration of all subjects in the OASIS database (150 subjects), comparing the average obtained via (a) MRI-based (single-channel) and (b) multistructure registration, both using locally optimal LDDMM registration. Registration performance can be assessed by whether the anatomical features are sharp (high accuracy) or blurred (low accuracy). We can see better definition of the cortical folding patterns with multistructure registration.

MRI image to compare residual variance for the multistructure and MRI-based registration approaches, as shown in Fig. 6.

4.3 Tensor-Based Morphometry

We tested for the effect of group using SurfStat with the linear model, $M = 1 + Group$, and examined differences be- tween nondemented (CDR = 0) and demented subjects (CDR = 0.5/1). Fig. 7 shows the T-statistics for the comparison of the demented group to the nondemented group,

showing greater differences in the medial temporal regions using the multistruc- ture approach. Fig. 8 shows the significant ($P < 0.05$) clusters of relative volume contraction in the demented group found by the MRI-based and multistructure groupwise registration meth- ods, with significance level correction using RFT. We see large significant clusters in the medial temporal lobe and hippocam- pus as detected by the multistructure registration, whereas the MRI-based registration detects a small cluster in the posterior

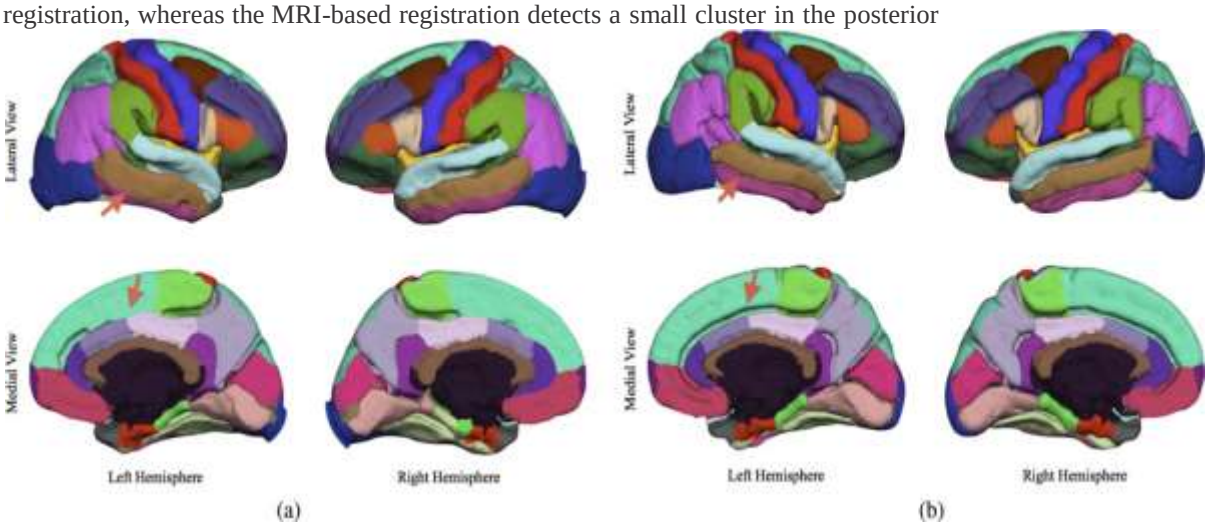

Fig. 5. Cortical surface reconstructions of the average MRI images generated using (a) MRI-based (single-channel) and (b) multistructure group-wise registration generated by Freesurfer. Cortical regions were labeled by surface-based registration to the Freesurfer cortical parcellation atlas. These visualizations show greater detail and consistency with expected cortical anatomy, demonstrating that the multi-structure registration aligns the cortical regions better than the MRI-based registration. (a) Cortical surface of MRI-based average. (b) Cortical surface of multistructure average.

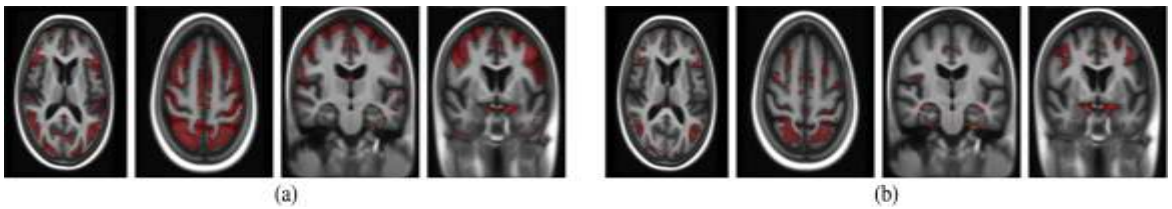

Fig. 6. Visualization of the residual variance from groupwise registration of all subjects in the OASIS database (150 subjects) comparing the (a) MRI-based approach (b) to the multistructure approach. The variance at each voxel was computed using the MRI image intensities of all subjects in the average space, and the visualization is showing the variance thresholded at $\sigma = 20$ to aid comparison. We see that the multistructure approach results in less overall residual variance, and that variance is generally greater in the posterior regions of the brain.

Cingulate gyrus. Both methods failed to detect any differences of relative volume expansion in the demented group.

V. DISCUSSION

Our multistructure framework has the significant advantage of being flexible enough to allow use of computed features derived from MRI images, such as white matter tract-based labels and diffusion tensor metrics or additional modalities such as BOLD functional images, susceptibility weighted images, magnetiza- tion transfer images, or quantitative relaxation-based maps. A multicontrast LDDMM approach specific to the problem of dif- fusion tensor image registration [30] has also been proposed. In this approach, whole brain registration was performed with diffusion-tensor derived images such as b_0 , fractional anisotropy (FA) and combined b_0 , and FA with the goal of better aligning whole brain white matter regions and ventricles for DTI nor- malization. The findings of this study are similar to ours in that the incorporation of multiple streams of information improves registration. Our approach of using multiple structure segmen- tations to drive local whole brain registration shows for the first time that, as expected, incorporation of individual segmentations into the registration further improves local registration accuracy. A drawback of this approach is the additional burden to provide initial structure segmentations; however, employing a tool such as FreeSurfer, which is highly automated, free, and commonly used in the neuroimaging community, this additional burden is placed on increased computational

time only. Group-wise registration approaches that solely use the MRI image intensities to generate an average template are suscepti- ble to partial volume effects that occur when intensities from different tissue types are averaged together as a result of mis- registration. This can lead to the generation of false anatomy, if for example, CSF intensities were averaged with WM in- tensities, the average obtained would be interpreted as a GM intensity. Our multistructure approach helps alleviate this prob- lem by using separate channels for each cortical gray-matter parcellation, such that when these are averaged together there is no partial-voluming of different tissue types. This effect could explain the much higher cortical registration accuracy seen with the group-wise multistructure approach. Previous studies on us- ing segmentation shape matching for cortical alignment, such as [2] also support this conclusion.

The combination of different structure segmentations in the whole brain registration as we have proposed allows the incor- poration of *a priori* relative weights reflecting confidence levels for variability of individual ROIs as well as confidence in seg- mentation accuracy. At this time, these weights are fixed to be equal; however, these could be optimized over a small train- ing database for best whole brain registration in a principled

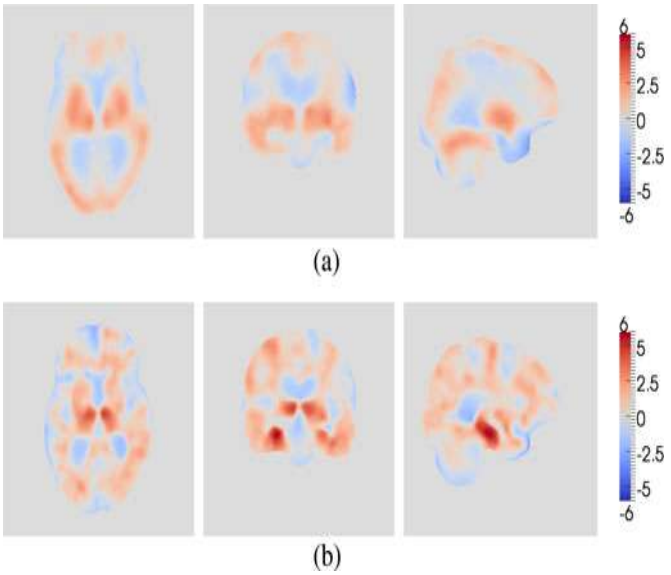

Fig. 7. T-statistic maps showing TBM-based group differences between non- demented and demented subjects in the OASIS database, comparing results from (a) MRI-based group-wise registration (b) to multistructure group-wise registration. Cool colors indicate regions where relative expansion is greater in demented subjects, and warm colors show where relative contraction is greater in demented subjects. We see relative expansion in the ventricles using both methods, and a high level of contraction in regions occupied by the hippocam- pus, thalamus, and medial temporal lobe detected by the multistructure method only.

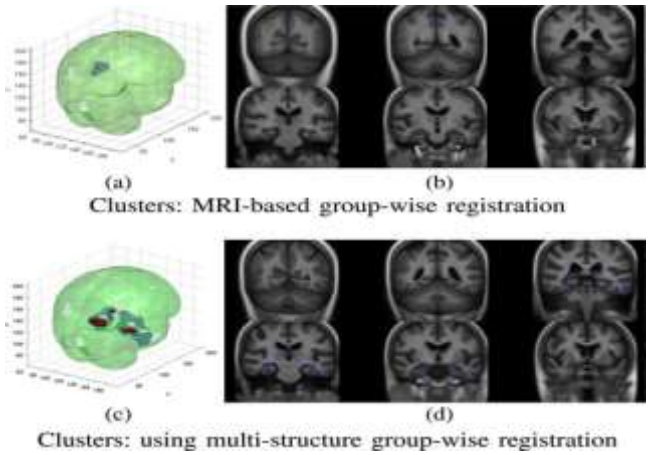

Fig. 8. Visualizations showing regions of significant ($P < 0.05$) TBM-based group differences between nondemented and demented subjects in the OASIS database, comparing results from (a) and (b) MRI-based group-wise registration to (c) and (d) multistructure group-wise registration. The surface visualizations, (a) and (c), depict significant regions of voxel-wise significance (red) and cluster- wise significance (blue). The orthoslice visualizations, (b) and (d), show the av- erage MRI overlaid with outlines surrounding all significant regions (both

voxel- wise and cluster-wise significant). These clusters relate to the positive T-statistics shown in Fig. 7, showing where demented subjects experience greater relative contraction than nondemented subjects. We see large clusters in the temporal lobe, hippocampus, and thalamus with the multistructure approach, and a single small cluster in the posterior cingulate with the MRI-based approach.

Way. Another approach would be to weigh the relative channel contributions of the segmentation channels to be inversely pro- portional to the size of the structures, so errors in alignment over smaller structures are penalized more heavily. In the evaluation of cortical overlap metrics, we had seen reduced performance of frontal lobe alignment with the multistructure approach. This could be due to the relatively larger size of Freesurfer corti- cal parcellations in the frontal region; if the parcellations are smaller, the effective correspondences through shape matching are at a finer scale. Conversely, if the parcellations are larger and encompass more cortical folding variability, their effectiveness is reduced since they would be more susceptible to local min- ima. Adaptive weighting of the structure channels could thus potentially aid in addressing this problem as well.

Another limitation of our approach is the large amount of computational resources required for multistructure registration. Although the computational time and memory requirements in- creases linearly with the number of structures, or channels, in the multistructure approach, we do, however, use a large number of structures for our brain registration, with 37 cortical parcella- tions and 8 subcortical structures. If we were to include further modalities, such as diffusion tensor or functional data, the total number of channels would further increase. Also, the FreeSurfer processing pipeline often takes several hours to complete corti- cal reconstruction and segmentation for a single brain. However, thanks to significantly increasing hardware capabilities in face of rapidly decreasing hardware costs, and to several national and international high-performance computing (HPC) initia- tives that now allow easy access to computational resources; the tradeoff between computational cost and enhanced accuracy of whole brain registration, as demonstrated in Figs. 1 and 2, is increasingly acceptable.

REFERENCES

[1]. A. R. Khan, L. Wang, and M. F. Beg, "Freesurfer-initiated fully-automated subcortical brain segmentation in MRI using large deformation diffeomor- phic metric mapping," *Neuroimage*, vol. 41, no. 3, pp. 735–46, 2008.

[2]. M. A. Yassa and C. E. Stark, "A quantitative evaluation of cross- participant registration techniques for MRI studies of the medial temporal lobe," *Neuroimage*, vol. 44, no. 2, pp. 319–327, 2009.

[3]. F. Wang and B. C. Vemuri, "Simultaneous registration and segmentation of anatomical structures from brain MRI," *Proc. SPIE*, vol. 8, pp. 17–25,

[4]. 2005.

[5]. K. M. Pohl, J. Fisher, W. E. L. Grimson, R. Kikinis, and W. M. Wells, "A bayesian model for joint segmentation and registration," *Neuroimage*, vol. 31, no. 1, pp. 228–39, 2006.

[6]. C. L. Guyader and L. Vese, "A combined segmentation and registration framework with a nonlinear elasticity smoother," *Comput. Vis. Imag. Un-*

[7]. *derstand.*, vol. 115, no. 12, pp. 1689–1709, 2011 B. Fischl, D. Salat, E. Busa, M. Albert, M. Dieterich, C. Haselgrove, A. van der Kouwe, R. Killiany, D. Kennedy, and S. Klaveness, "Whole brain segmentation: Automated labeling of neuroanatomical structures in the human brain," *Neuron*, vol. 33, no. 3, pp. 341–355, 2002.

[8]. G. Postelnicu, L. Zollei, and B. Fischl, "Combined volumetric and surface registration," *IEEE Trans. Med. Imag.*, vol. 28, no. 4, pp. 508–522, Apr. 2009.

[9]. C. Lederman, A. Joshi, I. Dinov, J. D. V. Horn, A. Garcia, K. Chan, L. Vese, and A. Toga, "Automatic structural brain registration using finite elements and active surfaces," Dept. Mathemat., Univ. California, Los Angeles., Comput. Appl. Mathemat. Rep. 10-82, pp. 1–18, 2010

[10]. J. Du, L. Younes, and A. Qiu, "Whole brain diffeomorphic metric mapping via integration of sulcal and gyral curves, cortical surfaces, and images," *Neuroimage*, vol. 56, no. 1, pp. 162–73, 2011.

[11]. A. Dale, B. Fischl, and M. Sereno, "Cortical surface-based analysis—Part I: Segmentation and surface reconstruction," *Neuroimage*, vol. 9, no. 2, pp. 179–194, 1999.

[12]. B. Fisch, M. I. Sereno, and A. M. Dale, "Cortical surface-based analysis— Part II: inflation, flattening, and a surface-based coordinate system," *Neu- roimage*, vol. 9, no. 2, pp. 195–207, 1999.

[13]. M. F. Beg, M. I. Miller, A. Trouvé, and L. Younes, "Computing large deformation metric mappings via geodesic flows of diffeomorphisms," *Int. J. Comput. Vis.*, vol. 61, no. 2, pp. 139–157, 2005.

[14]. G. E. Christensen, S. C. Joshi, and M. I. Miller, "Volumetric transforma- tion of brain anatomy," *IEEE Trans. Med. Imag.*, vol. 16, no. 6, pp. 864– 877, Dec. 1997.

[15]. J. P. Thirion, "Image matching as a diffusion process: An analogy with Maxwell's demons," *Med.*

Imag. Anal., vol. 2, no. 3, pp. 243–260, 1998. [15] D. Rueckert, L. I. Sonoda, C. Hayes, D. L. Hill, M. O. Leach, and D. J. Hawkes, "Nonrigid registration using free-form deformations: Ap- plication to breast MR images," *IEEE Trans. Med. Imag.*, vol. 18, no. 8, pp. 712–721, Aug. 1999.

[16]. G. E. Christensen, R. D. Rabbitt, and M. I. Miller, "Deformable templates using large deformation kinematics," *IEEE Trans. Imag. Process.*, vol. 5, no. 10, pp. 1435–1447, Oct. 1996.

[17]. B. Avants and J. C. Gee, "Geodesic estimation for large deformation anatomical shape averaging and interpolation," *Neuroimage*, vol. 23, no. Suppl 1, pp. S139–S150, 2004.

[18]. B. Davis, P. Lorenzen, and S. Joshi, "Large deformation minimum mean squared error template estimation for computational anatomy," in *Proc. IEEE Int. Symp. Biomed. Imag. Nano Macro*, Apr. 2004, vol. 1, pp. 173– 176.

[19]. S. Joshi, B. Davis, M. Jomier, and G. Gerig, "Unbiased diffeomorphic atlas construction for computational anatomy," *Neuroimage*, vol. 23, no. Suppl 1, pp. S151–S160, 2004.

[20]. P. Lorenzen, M. Prastawa, B. Davis, G. Gerig, E. Bullitt, and S. Joshi, "Multi-modal image set registration and atlas formation," *Med. Imag. Anal.*, vol. 10, no. 3, pp. 440–451, 2006.

[21]. J. Ashburner and K. J. Friston, "Computing average shaped tissue proba- bility templates," *Neuroimage*, vol. 45, no. 2, pp. 333–341, 2009.

[22]. J. Ma, M. I. Miller, A. Trouvé, and L. Younes, "Bayesian template estima- tion in computational anatomy," *Neuroimage*, vol. 42, no. 1, pp. 252–261,

[23]. 2008.

[24]. A. R. Khan, "Improving brain registration and segmentation using anatom- ical guidance," Ph.D. dissertation, School of Eng. Sci., Simon Fraser Univ., Burnaby, BC, Canada, pp. 1–186, 2011

[25]. D. W. Shattuck, M. Mirza, V. Adisetiyo, C. Hojatkashani, G. Salamon, K. L. Narr, R. A. Poldrack, R. M. Bilder, and A. W. Toga, "Construction of a 3D probabilistic atlas of human cortical structures," *Neuroimage*, vol. 39, no. 3, pp. 1064–1080, 2008.

[26]. A. Klein, J. Andersson, B. A. Ardekani, J. Ashburner, B. Avants, M.-C. Chiang, G. E. Christensen, D. L. Collins, J. Gee, P. Hellier,

[27]. J. H. Song, M. Jenkinson, C. Lepage, D. Rueckert, P. Thompson, T. Vercauteren, R. P. Woods, J. J. Mann, and R. V. Parsey, "Evaluation of 14 nonlinear deformation algorithms applied to human brain MRI reg- istration," *Neuroimage*, vol. 46, no. 3, pp. 786–802, 2009.

[28]. D. S. Marcus, A. F. Fotenos, J. G. Csernansky, J. C. Morris, and R. L. Buckner, "Open access series of imaging studies: Longitudinal MRI data in nondemented and demented older adults," *J. Cognit. Neurosci.*, vol. 22, no. 12, pp. 2677–2684, 2010.

[29]. B. Avants, C. Epstein, M. Grossman, and J. Gee, "Symmetric diffeomor- phic image registration with cross-correlation: Evaluating automated la- beling of elderly and neurodegenerative brain," *Med. Imag. Anal.*, vol. 12, no. 1, pp. 26–41, 2008.

[30]. B. A. Ardekani, S. Guckemus, A. Bachman, M. J. Hoptman, M. Wojtaszek, and J. Nierenberg, "Quantitative comparison of algorithms for inter-subject registration of 3D volumetric brain MRI scans," *J. Neu- rosci. Methods*, vol. 142, no. 1, pp. 67–76, 2005.

[31]. J. Ashburner, "A fast diffeomorphic image registration algorithm," *Neu- roimage*, vol. 38, no. 1, pp. 95–113, 2007.

[32]. C. Ceritoglu, K. Oishi, X. Li, M.-C. Chou, L. Younes, M. Albert, C. Lyketsos, P. C. M. van Zijl, M. I. Miller, and S. Mori, "Multi-contrast large deformation diffeomorphic metric mapping for diffusion tensor imaging," *Neuroimage*, vol. 47, no. 2, pp. 618–627, 2009.